accumulation of technetium-99m-glucarate and technetium-99m-gluconate by Chinese hamster ovary cells in vitro. *J Nucl Med* 1993;34:242–245.

22. Marshall RS, Koch CJ, Rauth AM. Measurement of low levels of oxygen and their effect on respiration in cell suspensions maintained in an open system. *Radiat Res* 1986;108:91–101.

23. Whillans DW, Rauth AM. An experimental and analytical study of oxygen depletion in stirred cell suspensions. *Radiat Res* 1980;84:97–114.

24. Bristow RG, Hardy PA, Hill RP. Comparison between in vitro radiosensitivity and in vivo response of murine tumor cell lines. I. Parameters of in vitro radiosensitivity and endogenous cellular glutathione levels. *Int J Radiat Oncol Biol Phys* 1990;18:133–145.

25. Taylor YC, Rauth AM. Differences in the toxicity and metabolism of the 2-nitroimidazole misonidazole (Ro07-0582) in HeLa and Chinese hamster ovary cells. *Cancer Res* 1978;38:2745–2752.

26. Koch CJ, Giandomenico AR, Iyengar CW. Bioreductive metabolism of AF-2[2-(2-furyl)-3-(5-nitro-2-furyl)acrylamide] combined with 2-nitroimidazoles. Implications for use as hypoxic cell markers. *Biochem Pharmacol* 1993;46:1029–1036.

27. Marshall RS, Rauth AM. Oxygen and exposure kinetics as factors influencing the cytotoxicity of porfiromycin, a mitomycin C analog, in Chinese hamster ovary cells. *Cancer Res* 1988;48:5655–5659.

28. Rauth AM, Marshall RS, Kuehl BL. Cellular approaches to bioreductive drug mechanisms. *Cancer Metastasis Rev* 1993;12:153–164.

29. Chan YW, Linder KE, Jayatilak PG, et al. In-vitro studies of the hypoxic retention of a novel technetium-99m labeled nitroimidazole in rat heart [Abstract]. *J Nucl Med* 1994;35:18P–19P.

30. McClelland RA, Panicucci R, Rauth AM. Products of the reduction of 2-nitroimidazoles. *J Am Chem Soc* 1987;109:4308.

31. Chapman JD, Ball K, Lee J. Characteristics of the metabolism-induced binding of misonidazole to hypoxic mammalian cells. *Cancer Res* 1993;43:1523–1528.

32. Kavanaugh M-C, Sun A, Hu Q, Hill RP. Comparing techniques of measuring tumor hypoxia in different murine tumors: Eppendorf pO_2 histograph, [³H]misonidazole binding and paired survival assay. *Radiat Res* 1996;145:491–500.

33. Grunbaum Z, Freauff SJ, Krohn KA, Wilbur DS, Magee S, Rasey JS. Synthesis and characterization of congeners of misonidazole for imaging hypoxia. *J Nucl Med* 1987;28:68–75.

34. Rumsey WL, Patel B, Linder KE. Effect of graded hypoxia on retention of technetium-99m-nitroheterocycle in perfused rat heart. *J Nucl Med* 1995;36:632–636.

Targeting of Glucose Transport Proteins for Tumor Imaging: Is It Feasible?

Carol Anne Nelson, Qian Jennifer Wang, Jeffrey Paul Bourque and Paul David Crane

DuPont Merck Pharmaceutical Company, North Billerica, Massachusetts

If glucose transport proteins (Glut) are elevated in tumors they may be good targets for tumor imaging. For targeting, the overexpression of Glut should be a general characteristic of tumors. Moreover agents which bind to Glut should accumulate selectively in tumors. **Methods:** To test this, we quantitated Glut in isolated membranes from three human tumor xenografts, two murine tumor models and normal murine tissues using direct binding studies. Additionally, the biodistribution of two compounds which bind to Glut, 7-[[2-(3-(¹²⁵I-p-hydroxyphenyl)propionyl)aminoethyl)amino]carbonyl]-7-desacetyl-forskolin ([¹²⁵I]HPP forskolin) and [³H]cytochalasin B, were studied in a tumor model which overexpressed Glut. **Results:** There were multiple classes of binding sites for [³H]cytochalasin B and a percentage of these sites were competitive with D-glucose but not L-glucose. The rank potency and IC_{50} values for [³H]cytochalasin B binding were: 2-deoxy-D-glucose (4.5 mM) ≥ D-glucose (7 mM) > mannose (25 mM) > galactose (35 mM) > rhamnose (1–3 mM) > sorbitol (1–3 mM) and were similar to reported values for transport. The average density of Glut in four tumor models and normal tissues was between 0.7 and 4 pmole/mg protein, but K_d values were not significantly different (69 nM). In LX-1 human lung tumor xenograft (LX-1) Glut were 10-to-20-fold higher than other tissues (21.6 ± 0.6 pmole/mg protein, p < 0.01). Immunostaining of Glut-1 was more prominent in LX-1 than other xenograft tumors, consistent with the binding data. Glut density was highest in poorly vascularized regions suggesting that Glut upregulation was related to a biofeedback mediated event. Iodine-125 HPP-forskolin and [³H]cytochalasin B did not localize in LX-1 tumors. **Conclusion:** Glut overexpression was not a common characteristic of the five tumors tested. Iodine-125 HPP-forskolin and [³H]cytochalasin B did not localize in LX-1 tumors, indicating that these agents did not target tumors with upregulated Glut. Results suggest that Glut are not a promising target for tumor imaging.

Key Words: glucose transport proteins; tumor imaging; PET

High glucose metabolism has long been recognized as a distinguishing characteristic of tumors. Historically, tumors placed in solution were found to take up large concentrations of glucose relative to normal tissues (*1*). The accumulation of 2-DG analogs such as [¹⁸F]FDG has been used to image tumors with PET (*2–4*). The phosphorylated form of [¹⁸F]FDG is trapped intracellularly because it is not a good substrate for cellular export or further metabolism (*5*). The high concentration of [¹⁸F]FDG in tumors has been attributed to increased hexokinase activity (*6*), decreased phosphatase activity (*5*) or high concentrations of Glut (*7–10*). In situ hybridization studies from several groups have shown overexpression of Glut mRNA and transcript in a variety of human primary tumors (*7,9–11*). In addition, several studies have linked the transformation of cells to a direct upregulation of Glut (*12–15*). From these studies, it is generally accepted that the upregulation of Glut is a common characteristic of tumor biology. It has been suggested that agents which bind to Glut, such as labeled 3-radio-iodo-phloretin, may serve as alternative tumor imaging agents to ¹⁸F-FDG (*16*). Dissociation constants for the binding of [¹²⁵I]HPP forskolin and [³H]cytochalasin B to Glut (100 nM) are higher than dissociation constants for phloretin (1 uM) (*16–18*), and thus chosen for this study. Two approaches were taken to determine whether Glut could be targeted for tumor imaging: (1) the concentrations of Glut were estimated in five tumors, and six normal tissues; and (2) the biodistribution of [¹²⁵I]HPP forskolin and [³H]cytochalasin B was measured in tumor xenografts that overexpressed Glut.

MATERIALS AND METHODS

Tumor Xenografts

Female Crl:CD-1®-nuBr outbred isolator maintained nude mice (10–12 wk old) were used for all human tumor xenografts. The MX-1 human breast carcinoma xenograft and the LX-1 human lung carcinoma xenograft were both established by B. Giovanella of the Stehlin Foundation of Houston, Texas. Xenografts were

passaged many years in the NCI screening panel of experimental tumors (19). The DLD-2 colon xenograft was established by Dexter et al. (20). All human tumor lines were passaged as subcutaneous implants in nude mice; fragments of tumors 3 × 3 mm in size were placed either unilaterally or bilaterally in the inguinal axillae of each animal.

Synthesis of Hpp-Forskolin

7-[[(2-Aminoethyl)amino]carbonyl]-7-desacetylforskolin was synthesized using a published procedure (17). ^{1}H NMR spectrum was recorded on a 270-MHz spectrometer in CDCl$_3$. Chemical shifts are reported in parts per million with peak multiplicities being indicated as follows: s = singlet; d = doublet; t = triplet; m = multiplet; dd = double of doublets. The following peak assignments were noted and correlated with the original published synthesis of this compound: 5.95 (dd, 1 H), 5.22 (d, 1 H), 5.20 (d, 1 H), 4.96 (d, 1 H), 4.54 (m, 2 H), 3.22 (d, 2 H), 2.88 (t, 2 H), 2.42 (d, 1 H), 2.16 (d, 1 H), 1.70 (s, 3 H), 1.42 (s, 3 H), 1.35 (s, 3 H), 1.24 (s, 3 H) and 1.02 (s, 3 H). Analytical thin-layer chromotography was performed on a silica gel plate. Visualization of the final amine was by trinitrobenzenesulfonic acid spray. R$_f$ = 0.33 (EtOAc/HOAc/H2O 8/1/1) Iodination of 7-[[(2-Aminoethyl)amino]carbonyl]-7-desacetylforskolin was carried out using the Bolton-Hunter reagent as described (17).

Membrane Preparation

Mice were killed by decapitation. The organs or tumors were minced and homogenized in 10 ml of 20 mM Tris-HCl, pH 7.5 containing 10 mM EDTA (4°C). A Brinkman Polytron with a small probe of a P10/35 (4.5 for 30 sec) was used for homogenization. The suspension was centrifuged at 48,000 × g for 10 min (4°C). The pellet was resuspended in 40 ml of assay buffer (Tris-HCl, pH 7.5) with the homogenizer (4 sec) and filtered through three layers of cheesecloth. Membranes were washed two times and the final pellet was resuspended in assay buffer (1 ml/100 mg of original organ or tumor weight). Protein was determined using procedure P 5656 (Sigma, St. Louis, MO).

Filtration Assay for Tritiated Cytochalasin B Binding

Membrane protein was incubated at 20°C with [^{3}H]cytochalasin B in 20 mM Tris-HCl, pH 7.5. Nonspecific binding was determined in the presence of 0.5 M 2-DG. Specific binding was determined in the presence of 0.5 M sorbitol. Cytochalasin E (10 μM) was included in the assay to decrease nonspecific binding. After a 30 min incubation the membrane protein was filtered through Whatman GF/C filter paper under reduced pressure and washed with 8 ml buffer (4°C) using a 24-probe Brandell Cell Harvester. The filters were assayed for tritium activity in a Packard liquid scintillation counter for 3 min in 10 ml Cytoscint (Fisher, Pittsburgh, PA).

Centrifugation Assay for Tritiated Cytochalasin B Binding

Filtration and centrifugation techniques for separating bound from free [^{3}H]cytochalasin B were run in parallel using the same membrane preparation. Prior to centrifugation or filtration, procedures were identical. Tubes were then centrifuged in a microfuge for 3 min and inverted over 20 ml scintillation vials. The pellet was dispersed with 100 μl sodium dodecyl sulfate (10% v/v in water), incubated at room temperature for 30 min and inverted over a fresh scintillation vial. Supernatants and solubilized pellets were assayed for tritium activity in 10 ml of Aquasol.

Biodistribution Studies

Mice were intravenously injected with 100 μl of saline containing 10 μCi labeled compound. At various times, animals were decapitated. Trunk blood was collected, and the organs were rinsed in saline and weighed. Muscle was from the *quadriceps femoris*. Gamma emitters were counted in a gamma counter. For tritium

labeled compounds organs were minced in a 20-ml glass scintillation vial and Solvable (Sigma) was used as directed. Samples were assayed for ^{3}H activity in 15 ml of acidified Aquasol (7.5 ml of glacial acetic acid/l).

Immunostaining

Tumors were embedded in Histoprep and frozen at −30°C. Embedded tumors were sliced in five micron sections using a Bright cryostat. Tumor sections were removed from the freezer and air dried for 20 min. Tumor sections were fixed in saline containing 4% paraformaldehyde for 5 min at 4°C. The slides were then placed in phosphate buffered saline (PBS) for 10 min, 0.3% H$_2$O$_2$ for 30 min, and PBS for 20 min. Tris buffered saline (TBS) containing 0.1% avidin was dropped onto the slices and incubated 20 min in humidified chambers. After a 10 min wash in TBS, a solution of TBS containing 0.01% biotin was dropped onto tumor slices and incubated for 20 min. After another 10 min wash in TBS, normal blocking serum was added dropwise onto tumor slices and incubated 20 min following the directions from the Vector Elite ABC kit (Burlingham, CA) to the peroxidase step. Peroxidase substrate from ABC kit was incubated 2 min.

In some experiments, tumors were fixed in 10% buffered formalin for 24 hr and embedded in paraffin before slicing. Positive controls for Glut-1, Glut-3 and Glut-5 were caco cell smears. Positive controls for Glut-2 and Glut-4 were murine liver smears. Red blood cells contain only Glut-1 and were used to assess the degree of cross reactivity of antibodies against Glut-2 through Glut-5 with Glut-1. The purity of the red cell preparation was confirmed by microscopy. Similar controls are not available for antibodies directed against Glut-2 through Glut-5, since most tissues contain some Glut-1 (21). Excess antigen for Glut-1 (5 μg) was used in some experiments to block the immunostaining of Glut-1 in LX-1, and MX-1 tumor slices and demonstrate specificity.

Cellular Necrosis and Heterogeneity

Tumors were fixed in 10% buffered formalin and sectioned (5 microns). Tumors with similar weights (0.3 g) were compared. Hematoxylin and eosin (H&E) staining were carried out as described previously (22). Photographs of H&E stained sections were taken of the top and bottom of a slice every 25 microns into the tumor at a 40x magnification. Thirty-eight photographs of each tumor were analyzed. The area of necrotic tissue, viable tumor tissue and nontumor cells in each photograph was assessed. All areas for the 38 photographs were then averaged.

Statistical Methods

Data are expressed as mean ± s.e.m. Least squares analysis of Scatchard plots were computed and graphed using KaleidaGraph version 2.0. B$_{max}$ and K$_d$ values were calculated from Scatchard plots (23). Curve fitting analysis of multiphasic binding isotherms were done using LIGAND. Multiple comparisons were done using ANOVA followed by Kneuman Kuels test and the comparison of large and small tumors were done using a Student's t-test.

RESULTS

Homogenization, Filtration and Incubation

The stability of the Glut binding sites during assay procedures was measured. Tritium cytochalasin B binding reached equilibrium by 5 min at 20°C, and more rapidly at 30°C in the presence of 0.5 M sorbitol. Binding was stable to 90 min at both temperatures (data not shown). The effect of prolonged homogenization on Glut site density in membranes from LX-1 was also tested. Membranes from LX-1 were homogenized for 15 sec intervals and then assayed for Glut. The number of binding sites for [^{3}H]cytochalasin B was constant over 70 sec (data not
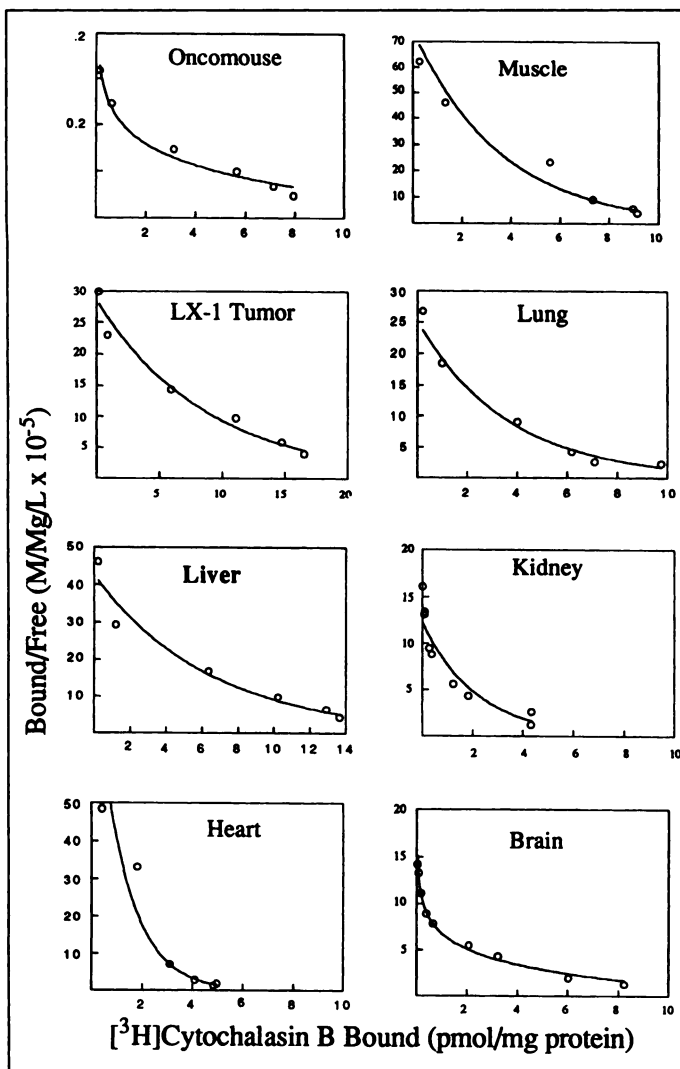
FIGURE 1. Scatchard plots of [³H]cytochalasin B binding in membrane preparations. Tritiated cytochalasin B was incubated in a Tris-HCl, pH 7.5, with and without excess cytochalasin B (10 μM) for the times indicated. Data are mean values of triplicate determinations representative of 3-to-8 experiments.

shown). Only 30 sec were required for membrane preparation. Centrifugation has been commonly used to separate bound from free [³H]cytochalasin B in whole cell and membrane systems (*18*). The centrifugation and filtration methods of separating membrane-bound from free [³H]cytochalasin B were compared at different concentrations of [³H]cytochalasin B in murine liver membranes. The nonspecific binding was decreased more than 50% in the filtration assay with no change in the number of specific binding sites at any of the concentrations tested (data not shown).

Cytochalasin B Displaceable Binding

Specific binding sites for [³H]cytochalasin B were measured by subtracting nonspecific binding in the presence of excess cytochalasin B from total binding in the absence of cytochalasin B (Fig. 1). The curves were multiphasic, indicating multiple classes of binding sites. Tritium cytochalasin B has been reported to bind to multiple classes of high affinity binding sites including Glut (*18*). B_{max} values were estimated by extrapolation and summarized in Table 1 and the range of B_{max} values for [³H]cytochalasin B was between 9 and 25 pmole/mg protein.

TABLE 1

Cytochalasin B Binding Parameters in Membranes from Tumors and Normal Tissues

	B_{max}, CB (pmole/mg protein)	B_{max}, Glut (pmole/mg protein)	Kd, Glut (nM)*
LX-1 lung, human xenograft	24.7	21.6 ± 0.6†	138 ± 16
MX-1 breast, human xenograft	11.65	1.14 ± 1.8	139 ± 25
DLD-2 colon, human xenograft	nd	2.75 ± 0.8	129 ± 25
B16 murine melanoma	nd	2.55 ± .8	77 ± 24
c-neu OncoMouse™, breast tumor	9.9	0.78 ± 0.6	26 ± 19
Murine brain	11.6	2.66 ± 0.6	60 ± 17
Murine liver	18.4	1.22 ± 0.8	13 ± 25
Murine heart	8.6	2.4 ± 0.7	49 ± 22
Murine lung	25.3	3.0 ± 1	17 ± 30
Murine kidney	9.1	3.5 ± 0.5	38 ± 16
Murine skeletal muscle	13.5	2.7 ± 0.8	74 ± 25

*K_d values were not significantly different from each other.
†$p < 0.01$ compared to other B_{max} using ANOVA and Kneuman Kuels.
Data are mean ± s.e.m., n = 3 to 8.
Glut = glucose transport proteins; CB = cytochalasin B; nd = not done.

D-Glucose Displaceable Binding

Glut have been measured directly using d-glucose to inhibit specific binding (*18,24*). In this way the non-Glut binding sites for cytochalasin B can be subtracted from the total. A percentage of the specific binding sites for [³H]cytochalasin B were competitive with d-glucose (Fig. 2, Table 1). L-glucose had no effect. Cytochalasin E decreased the nonspecific binding, possibly due to the inhibition of cytoskeletal interactions (*18*) with no change in the specific binding (data not shown). The inhibition of [³H]cytochalasin B binding by d-glucose was maximal at 0.5 M. Representative Scatchard plots of the glucose displaceable [³H]cytochalasin B binding sites in different membrane preparations are shown in Figure 2. Scatchard plots were linear indicating a single class of binding sites.

K_d values were not significantly different from one another in any group. The average K_d value for [³H]cytochalasin B binding to Glut was not significantly different from values in membranes from human red blood cells (data not shown) and Erlich ascites tumor cells in which direct binding studies with [³H]cytochalasin B are most commonly done (*18,24*). Normal tissues including murine brain, heart, lung, liver, kidney and skeletal muscle had site densities that ranged from 1.2-to-3.5 pmole/mg protein. The Glut site densities in other tumor models including LX-1, MX-1, DLD-2, B-16 and breast tumors from the c-neu OncoMouse™ are also shown. Membranes from the LX-1 tumor had B_{max} values for Glut 10-to-20-fold higher than all others (p < 0.01). Only LX-1 had Glut concentrations significantly higher than normal tissues.

In LX-1 membranes, 87% of the cytochalasin B displaceable binding sites were glucose displaceable. In other tissues, the percentage of glucose displaceable binding ranged from 10% to 30% of the cytochalasin B displaceable binding sites (Table 1). To characterize the inhibition of cytochalasin B by d-glucose, saturation isotherms were carried out at two concentrations of glucose (0.5 M and 0.02 M) using membranes from LX-1 tumors (Fig. 3). Increasing the concentration of glucose increased the apparent K_d with no change in the B_{max} value. This is characteristic of competitive inhibition.
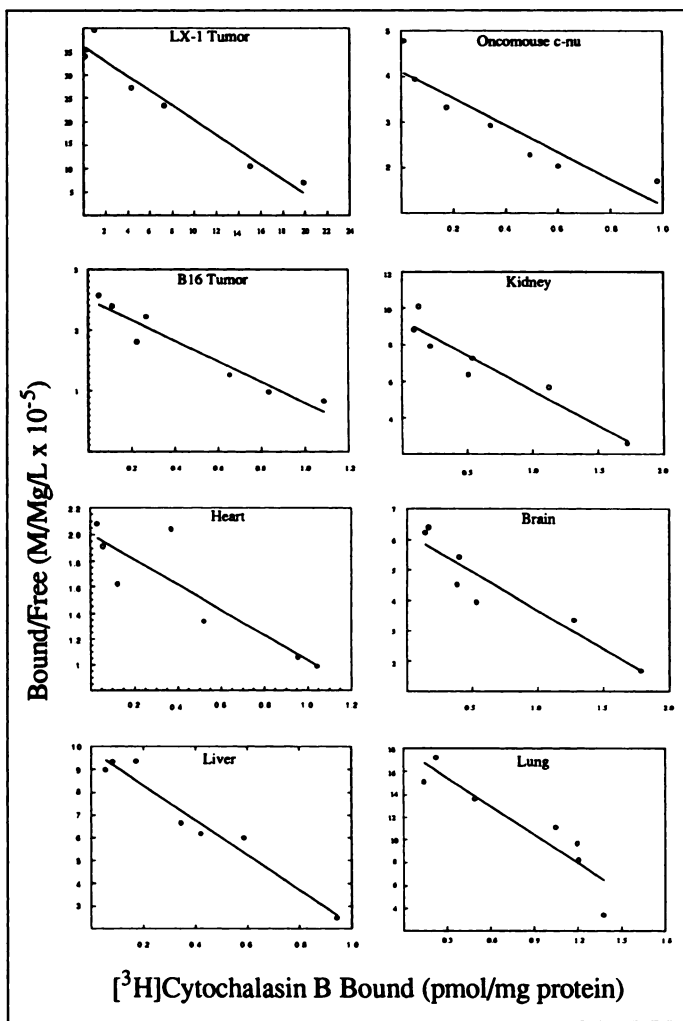
FIGURE 2. Scatchard plots of [³H]cytochalasin B binding to glucose transport proteins in membrane preparations. Tritium cytochalasin B was incubated in a Tris-HCl buffer solution at pH 7.5 containing cytochalasin E (10 μM) and either sorbitol (0.5 M), or 2-deoxy-D-glucose (0.5 M) for 20 min. Assays were filtered through GF/C filter paper under reduced pressure and counted. Data are mean values of triplicate determinations (n = 3 to 8). Parameters for pooled data are given in Table 1.
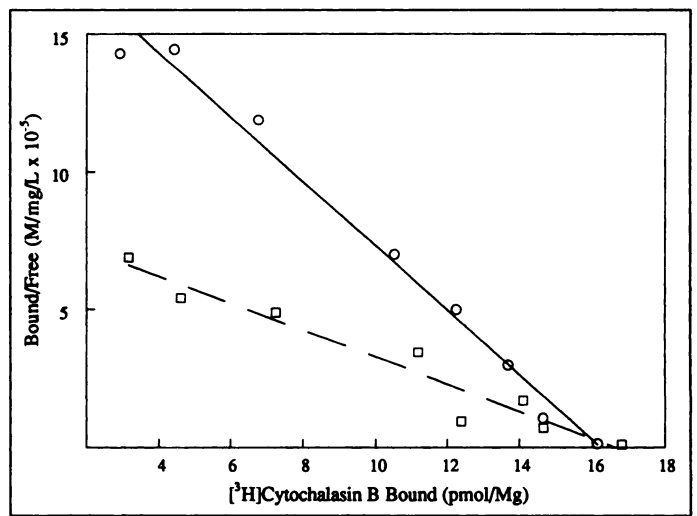

FIGURE 3. Competitive inhibition of [³H]cytochalasin B by D-glucose. Scatchard plots of the glucose displaceable binding of [³H]cytochalasin B to membranes from LX-1 tumor. Membrane protein was incubated with different concentrations of [³H]cytochalasin B. The nonspecific binding was measured in the presence of 10 μM cytochalasin E and 0.02 M (circles) or 0.5 M (squares) D-glucose as shown. The total binding was measure with 10 μM cytochalasin E and 0.5 or 0.02 M sorbitol. Specific binding was calculated by subtracting the nonspecific from the total binding.

Rank Potency of Sugar Transport Compared to Binding

The percent inhibition of [³H]cytochalasin B binding by different sugars was assessed to determine whether binding occurred in the same concentration range as transport (Fig. 4). The rank potency of competition for [³H]cytochalasin B binding sites in LX-1 membranes was d-glucose ≥ 2-deoxyglucose > mannose > galactose > rhamnose > sorbitol. This is the same rank potency reported for the inhibition of [³H]cytochalasin B binding to Glut in human erythrocytes (24) and erythrocyte membranes (25). The IC₅₀ values calculated from the inhibition curves are given in Table 2. Reported values for the inhibition of sugar transport in human red blood cells (26) are shown. IC₅₀ values for sugar transport across the blood brain barrier in rat are similar to those shown in Table 2 (27). Thus, different sugars compete for binding of [³H]cytochalasin B in LX-1 membranes over similar concentration ranges as they compete for transport in other systems (Table 2).

Effect of Tumor Size on Glut Density

To determine the effect of tumor size on Glut site density, large and small LX-1 tumors were compared (Table 3). Small tumors (<0.3 g) had 24 pmole Glut per mg protein compared to large tumors (>1.0 g) which had 15 pmole Glut per milligram protein. K_d values were not significantly different, and the yield

of membrane protein was the same in all tumors (4% of the original weight). Thus, small tumors had 29% higher Glut per milligram protein than large tumors (p < 0.01). Even the largest LX-1 tumors, however, had site densities of Glut at least 5-fold higher than membrane preparations from other tumor types.

Biodistribution Studies

The biodistribution of [³H]cytochalasin B, [¹²⁵I]HPP-forskolin, [³H]2-deoxyglucose and [¹²⁵I]IUDR was tested in the LX-1 tumor model. Optimal time points are shown in Table 4. The concentration of [³H]cytochalasin B and [¹²⁵I]HPP-forskolin in the tumors was below blood levels at 30, 60 and 120 min postinjection. The percent id/g of 2-deoxyglucose in tumor was higher than blood values at all time points tested. Similarly, [¹²⁵I]IUDR (known to target dividing cells) was markedly elevated in the LX-1 tumor compared to blood and other organs 24 hr after injection.
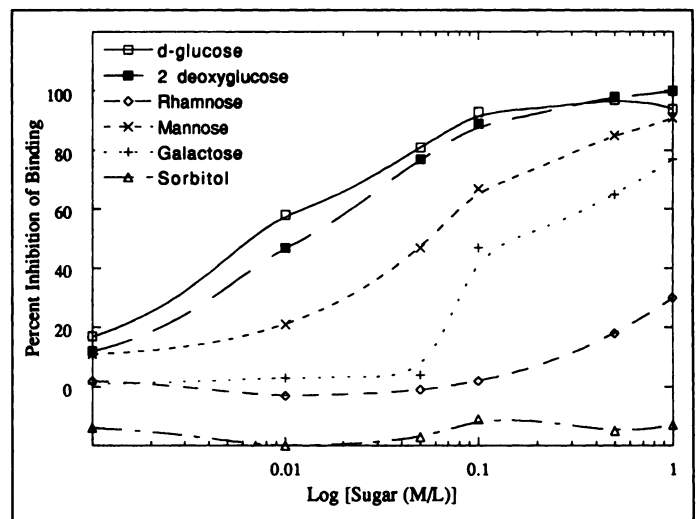

FIGURE 4. Rank potency competition of [³H]cytochalasin B binding. LX-1 membranes were incubated with [³H]cytochalasin B (50 nmole/l), cytochalasin E (10 μM), and concentrations of the sugars indicated for 30 min at 20°C. The values are the average of two separate experiments done in triplicate. The IC₅₀ values are given in Table 3.

Immunostaining Experiments

The expression of Glut isoforms 1–5 in LX-1 and MX-1 was measured using immunostaining techniques. Antibodies directed against human Glut-1, Glut-2, Glut-3, Glut 4 and Glut 5 were used. Initial studies showed some nonspecific staining in the MX-1 tumor slices without antibody. This nonspecific staining was not observed after preincubation of tumor slices with avidin and biotin. Strong staining of positive controls verified that each antibody was able to react with a tissue known to contain the transport protein against which it was directed. This staining was associated with the cell membranes in tumor slices. No detectable staining was seen in either tumor or red blood cell membranes using an antibody directed against Glut 3. Some weak staining was seen in both tumors using antibodies directed against Glut-2. Faint staining was apparent in both tumors using antibodies directed against Glut-4 and Glut-5. Staining in red blood cell membranes using antibodies directed against Glut-2, Glut-4 and Glut-5 was similar to that seen in the tumor slices (data not shown).

The immunostaining of Glut-1 was much higher in the LX-1 tumor compared to MX-1, and DLD-2 (Fig. 5 A–D). In all three tumors excess unlabeled antigen (Glut-1 peptide) was able to inhibit staining (data not shown). Strong positive staining was also observed in poorly vascularized regions (Fig. 5). In some experiments, 1:50 dilution of antibody was used to stain MX-1 and DLD-2 tumors. The same pattern of high staining was seen in poorly vascularized regions of MX-1 and DLD-2 (data not shown).

Histology

Tumors fixed in 10% buffered formalin before slicing had more distinct histological structures than tumor that had been sliced frozen and then fixed. Consequently, the regions of necrosis and cellular heterogeneity were performed on formalin-fixed tumors. The percentage of connective tissue, fat and red blood cells was less than 5% of the total cell population in LX-1, MX-1 and DLD-2 tumors. The percentage of necrotic regions was assessed microscopically after H&E staining. The percentage of necrotic regions was 16% in LX-1 and MX-1 and 37% in DLD-2.

DISCUSSION

Purpose

Evidence that Glut are overexpressed in tumors includes reports of elevated transcript and mRNA for Glut in fixed tumor slices and transformed cell lines. Tumors from liver (11), brain (9), the digestive system (10) and head and neck (28) have been reported to have high levels of Glut mRNA compared to normal tissues. Elevated Glut transcript in human tumors of the breast (7), brain (9) and head and neck (28) has been shown by immunohistochemical staining. Transformation of some cells with src, ras (13) and fps (12) have been linked to the increased synthesis and expression of Glut. Transformation with rous sarcoma virus has been linked to the upregulation of Glut before enhanced growth (29). 2-DG analogs such as [18F]FDG are transported into cells by Glut and are retained in tumors at high concentrations. These data imply that Glut overexpression is a general characteristic of tumor biology. Thus, it has been suggested that agents which bind to Glut may serve as alternative tumor imaging agents to [18F]FDG (16). To test the feasability of this hypothesis, we quantitated Glut in tumors and normal tissues.

Quantification of Glut

Glut were measured by direct binding and immunostaining techniques. [3H]cytochalasin B binds directly to Glut and has been used to quantitate Glut in red blood cells (30), Erlich Ascites tumor cells (18), adipose cells (31), rat liver membranes (32) and membranes from cerebral microvessels (33). The binding of [3H]cytochalasin B to membrane preparations was measured in the presence and absence of excess 2-DG. Two observations confirmed that specific binding sites were Glut: (1) D-glucose but not L-glucose competitively inhibited the binding of cytochalasin B (Figs. 2, 3); and (2) The inhibition of cytochalasin B binding by different sugars occurred in the same concentration range as their transport (Fig. 4). The concentration of Glut in normal tissues ranged from 2-to-4 pmole/mg protein. The concentration of Glut in four tumors ranged from 0.8-to-3 pmole/mg protein and was not different from normal tissues. In LX-1, Glut were 10-to-20-fold higher than normal tissues and other tumors (Table 1). Since LX-1 tumors stained intensely compared to MX-1 and DLD-2, immunostaining results were consistent with the binding data. Thus, only one of five tumors had concentrations of Glut significantly higher than normal tissues, a trend which appeared to contradict published reports of Glut density in human primary tumors (7,9,10,13,28).

Xenograft passage, tissue preparation, cellular heterogeneity and tumor necrosis are potential explanations for the apparent low expression of Glut in four out of five tumors. For example, Glut expression in a population of passaged tumors may not represent expression in primary tumors. Tumors from the c-neu OncoMouse™, however, were also studied. These transgenic animals develop tumors spontaneously (34), and were found to have low Glut (Table 1). Thus, a mutational artifact of xenograft passage was not a likely explanation. It was also unlikely that Glut degradation was occurring during filtration, homogenization or incubation procedures since Glut were found to be stable under these conditions. The percentage of necrotic zones were calculated in all xenografts and were found to be identical in LX-1 and MX-1 tumors (16%). In DLD-2 tumors 38% of the tumor was necrotic. The percentage of nontumor cells was found to be less than 5% in all three xenografts (Table 5). Correction for necrosis or cellular heterogeneity did not indicate Glut overexpression in DLD-2 or MX-1 relative to normal tissues. Thus, low Glut expression in four out of five tumors did not appear to be due to artifacts of cellular heterogeneity, necrosis, tissue preparation or xenograft passage.

Regional upregulation of Glut might lead to higher estimates of Glut when tumor slices are compared to homogenates of whole tumors. Immunostaining is the technique most often used to demonstrate overexpression of Glut in tumors (7,9,10,13,28). Tumors have hypoxic zones of low blood flow and these zones often become necrotic (35,36). Lower concentrations of Glut per milligram protein were found in large compared to small LX-1 tumors (Table 3). While large tumors have more necrotic zones (35,36) and may have similar protein concentrations they have less Glut per milligram of protein. We also observed that overexpression of Glut was most extensive in poorly vascularized regions (Fig. 5). It could be that cells near necrotic zones have high concentrations of Glut and zones of coagulation necrosis have lost their Glut. It is also possible that cells in necrotic zones may still retain epitopes of Glut which are no longer functional. Thus, immunostaining and binding could appear to give different results due to regional variations of Glut expression.

Glut concentration can be regulated by biofeedback and transformation-related events. Low levels of glucose and ATP can lead to the upregulation of Glut in cultured cells (37,38). Thus, conditions of low glucose and ATP occur in tumors (39). As stated previously, we observed that the upregulation of Glut

TABLE 2
Inhibition of Transport and Tritiated Cytochalasin B Binding by Different Sugars

Sugar	IC_{50} transport*	IC_{50}[^{3}H]CB binding†
2-deoxyglucose	4.5 mM	12.0 mM
d-glucose	7 mM	6.5 mM
d-mannose	25 mM	54.0 mM
d-galactose	35 mM	162.0 mM
d-rhamnose	>1 M	>1 M

*IC_{50} values for binding were calculated from inhibition curves (Fig. 5).
†Published values for the inhibition of glucose transport in red blood cells (26).

was most extensive in regions of low vascularization. A similar pattern of Glut expression has been observed in brain tumors (9), and human mammary tumors (7). In this study, immuno-staining techniques revealed that tumor cells adjacent to blood vessels in LX-1, DLD-2 and MX-1 all had similar staining intensity for Glut-1. LX-1, MX-1 and DLD-2 all had higher expression of Glut-1 in poorly vascularized regions. The staining of LX-1 was the most intense (Fig. 5 A–D). It is possible that LX-1 tumor cells express more Glut under stress than cells in the other tumors. A transformation-specific upregulation of Glut should occur uniformly throughout the tumor and be apparent on cells adjacent to blood vessels. Biofeedback mediated upregulation of Glut would be expected to occur in poorly vascularized regions. Thus, it appeared that Glut were upregulated in a biofeedback mediated response in all tumor xenograft models and that this response was more extensive in LX-1.

There are five isoforms of Glut which have been sequenced and characterized. Isoforms 1 and 3 are most commonly upregulated in tumors (7,9,11). With antibodies directed against isoforms 1–5 we found that only Glut-1 were significantly expressed in LX-1 and MX-1 tumors. DLD-2 also expressed Glut-1. Only human xenograft tissues were tested because the antibodies available were directed against human Glut. Excess antigen was able to inhibit staining, indicating the Glut-1 antibody had a specific interaction with Glut-1.

Tumor Targeting

LX-1 appeared to be an excellent model to determine whether targeting Glut in tumors would lead to high retention of agents which bind to Glut. Thus, the biodistribution of agents which bind to Glut such as [^{125}I]HPP-forskolin and [^{3}H]cytochalasin B was measured in LX-1. Agents known to target tumors such as [^{3}H]2-DG and [^{125}I]iododeoxyuridine (IUDR) were studied for comparison. The concentration of [^{3}H]-2-DG in LX-1 was well above blood values at all time points. Tumor-to-blood ratios in [^{125}I]IUDR treated animals were high indicating that

TABLE 3
Glucose Transport Protein Site Density in Large and Small LX-1 Tumors

Tumor weight (g)	No.	B_{max}, Glut (pmole/mg protein)	K_d, Glut (nM)	Membrane protein (mg/100 mg tissue)
1.39 ± 0.13	5	14.6 ± 1.8*	105 ± 11	4.3 ± 0.18
0.27 ± 0.12	6	23.8 ± 1.6†	101 ± 10	4.0 ± 0.16

*Significantly different from †, p < 0.01.
Data are mean ± s.e.m.
Glut = glucose transport proteins.

TABLE 4
Biodistribution of Tritiated Cytochalasin B, Iodine-125-HPP-forskolin, Iodine-125-UDR and Tritiated FDG in LX-1 Tumor Xenograft

Organ	% ID/g			
	CB (2 hr)	FSK (1 hr)	2-DG (0.5 hr)	IUDR (24 hr)
Blood	0.51 ± 0.03	0.49 ± 0.04	0.52 ± 0.06	0.058 ± 0.04
Brain	0.21 ± 0.03	0.05 ± 0.02	2.97 ± 0.29	0.07 ± 0.03
Heart	1.53 ± 0.29	0.98 ± 0.38	21.68 ± 1.78	0.061 ± .03
Lung	0.46 ± 0.05	0.45 ± 0.04	1.69 ± 0.09	0.14 ± 0.05
Liver	1.75 ± 0.38	0.88 ± 0.16	0.74 ± 0.09	0.33 ± 0.08
Gallbladder	59.9 ± 65.3	4949 ± 3085	0.91 ± 0.05	nd
Kidney	0.64 ± 0.01	0.59 ± 0.05	1.61 ± 0.11	0.18 ± 0.05
Muscle	2.58 ± 1.27	0.48 ± 0.41	0.97 ± 0.23	0.072 ± 0.03
Fat	0.7 ± 0.09	0.36 ± 0.05	0.38 ± 0.16	nd
Small intestine	8.23 ± 6.46	0.29 ± 0.04	1.75 ± 0.07	nd
LX-1 tumor	0.41 ± 0.05	0.48 ± 0.01	2.41 ± 0.12	1.06 ± 0.11

Data are mean ± s.e.m., n = 3.
nd = not done; CB = cytochalasin B; IUDR = iododeoxyuridine; HPP-FSK = 7-[[2-(3-(I125-p-hydroxyphenyl)propionyl)aminoethyl)amino]carbonyl]-7-desacetylforskolin; 2-DG = 2-deoxy-D-glucose.

LX-1 retained compounds known to localize in tumors. Tumor-to-blood ratios for [^{3}H]cytochalasin B were low. Since [^{3}H]cytochalasin B may have interacted with other high affinity sites besides Glut (Table 1) it was possible that a more specific agent was needed for selective targeting of tumors. Iodine-125-HPP-forskolin has higher specificity for Glut (17) than [^{3}H]cytochalasin B. Thus, we measured the biodistribution of [^{125}I] HPP-forskolin in LX-1. [^{125}I]HPP-forskolin and [^{3}H]cytochalasin B had similar percent id/g in the tumors when blood values were 0.5% id/g (Table 4). Tumor-to-muscle ratios were higher in animals injected with [^{125}I]HPP-forskolin, reflecting the higher specificity of this agent. The blood-to-tumor, ratios however, were low in both groups (Table 4). It is possible that agents with higher affinity for Glut are necessary for targeting the glucose binding sites. Clearly, intracellular trapping of agents like [^{3}H]-2-DG and [^{125}I]IUDR is an advantage for tumor targeting. Iodine-125 HPP-Forskolin and [^{3}H]cytochalasin B bind to Glut
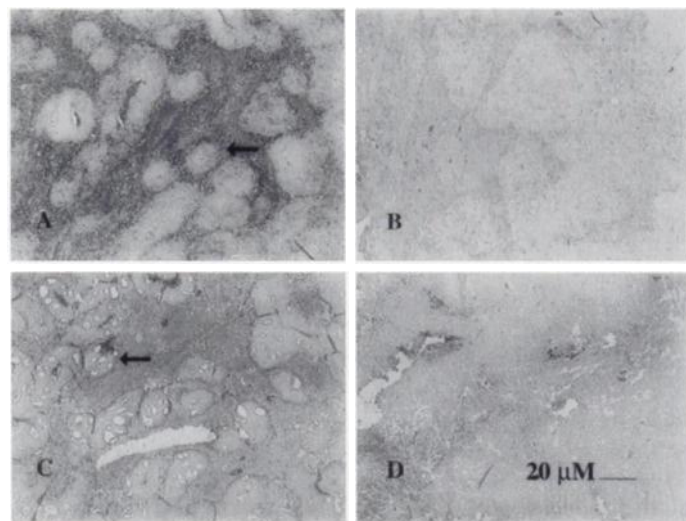

FIGURE 5. The expression of Glut-1 in tumor slices from LX-1, MX-1 and DLD-2 human tumor xenografts. Sections were immunostained with a 1:500 dilution of antibody as described in methods (X40). (A) Glut-1 positive staining of LX-1 tumor section (B) LX-1 incubated with healthy rabbit antiserum instead of Glut-1 antibody (C) Glut-1 positive staining in DLD-2 (D) Glut-1 positive staining in MX-1. Arrows show examples of blood vessels.

TABLE 5
Necrotic Zones and Nontumor Cells in Tumor Xenograft Models

Tumor xenograft	% Necrosis	% Nontumor cells
LX-1 lung, human	16 ± 3	5 ± 3
MX-1 breast, human	16 ± 5	1 ± 1
DLD-2 colon, human	38 ± 5	1 ± 1

Data are mean ± s.e.m. of 38 regions from each tumor.

but are not trapped intracellularly. The targeting of tumors [^{125}I]HPP-forskolin and [^{3}H]cytochalasin B agents relies primarily on their dissociation constant (about 100 nM) and the accessibility of Glut. It is not clear that the all of the Glut in tumors were accessible to these compounds, since most Glut were in zones of low blood flow. Additionally, it is possible that epitopes of Glut in necrotic zones recognised by Glut antibodies may have nonfunctional binding sites. Although agents with higher affinity for Glut might enhance the success of Glut targeting, this study suggests that targeting Glut in tumors may not be a good method for diagnostic imaging.

CONCLUSION

Glut were measured in normal tissues and tumors by direct binding and immunostaining techniques. We found that:

1. Glut were overexpressed in only one of five tumors.
2. Overexpression of Glut in LX-1 was 10–20-fold higher than other tumors and normal tissues.
3. Glut expression was highest in poorly vascularized regions.
4. Cells adjacent to blood vessels in all three xenograft models had similar Glut expression.
5. Iodine-125-HPP-Forskolin and [^{3}H]cytochalasin B were unable to target Glut in LX-1 tumors.

ACKNOWLEDGMENTS

REFERENCES

1. Warburg O. On the origin of cancer cells. *Science* 1956;123:309–314.
2. Coleman RE. Single-photon emission tomography in cancer imaging. *Cancer* 1991; 67:1261–1270.
3. Di Chiro G, De Le Paz RL, Brooks RA, et al. Glucose utilization of cerebral gliomas measured by ^{18}F-fluorodeoxyglucose and PET. *Neurology* 1982;32:1323–1329.
4. Hawkins RA, Phelps ME. Applications of PET in clinical oncology. *Cancer Metastasis Rev* 1988;7:119–142.
5. Gallagher BM, Fowler JS, Gutterson NI, MacGregor RR, Wan C, Wolf AP. Metabolic trapping as a principle of radiopharmaceutical design: some factors responsible for the biodistribution of [^{18}F] 2-deoxy-2-fluoro-D-glucose. *J Nucl Med* 1978;19:1154–1161.
6. Monakhov NK, Neistadt EL, Shaviovskli MM, Shvartsman AL, Neifakh SA. Physio-chemical properties and isoenzyme composition of hexokinase from normal and malignant human tissues. *J Natl Cancer Inst* 1978;61:27–33.
7. Brown RS, Wahl RL. Overexpression of GLUT-1 glucose transporter in human breast cancer. An immunohistochemical study. *Cancer* 1993;72:2979–2985.
8. Hatanaka M, Augl C, Gilden RV. Evidence for a functional change in the plasma membrane of murine sarcoma virus-infected mouse embryo cells. Transport and transport-associated phosphorolation of ^{14}C-2-deoxy-D-glucose. *J Biol Chem* 1970; 245:714–717.
9. Nishioka T, Oda Y, Seino Y, et al. Distribution of the glucose transporters in human brain tumors. *Cancer Res* 1992;52:3972–3979.
10. Yamamoto T, Seino Y, Fukumoto H, et al. Overexpression of facilitative glucose transporter genes in human cancer. *Biochem Biophys Res Commun* 1990;170:223–230.
11. Su T, Tsai T, Chi C, Han S, Chow C. Elevation of facilitated glucose-transporter messenger RNA in human hepatocellular carcinoma. *Hepatology* 1990;11:118–122.
12. Birnbaum MJ, Haspel HC, Rosen OM. Transformation of fibroblasts by FSV rapidly increases glucose transporter gene transcription. *Science* 1987;235:1495–1498.
13. Flier JS, Mueckler MM, Usher P, Lodish HE. Elevated levels of glucose transport and transporter messenger RNA are induced by ras or src oncogenes. *Science* 1987;235: 1492–1497.
14. Salter DW, Weber MJ. Glucose-specific cytochalasin B binding is increased in chicken embryo fibroblasts transformed by rous sarcoma virus. *J Biol Chem* 1979;254:3554–3561.
15. Weber G. Enzymology of cancer cells. *N Engl J Med* 1977;296:541–551.
16. Mertens J, Terriere D. 3-Radioiodo-Phloretin, A new potential radioligand for in vivo measurement of GLUT proteins: a spect alternative for ^{18}F-FDG. *J Nucl Biol Med* 1993;37:158–159.
17. Robbins JD, Laurenza A, Kosley RW, O'Malley GJ, Spahl B, Seamon KB. (Amino-alkyl)carbamates of forskolin: intermediates for the synthesis of functionalized derivatives of forskolin with different specificities for adenylyl cyclase and the glucose transporter. *J Med Chem* 1991;34:3204–3212.
18. Cuppoletti J, Mayhew E, Jung CY. Cytochalasin B binding to Ehrlich ascites tumor cells and its relationship to glucose carrier. *Biochim Biophys Acta* 1981;642:392–404.
19. Goldin A, Venditti JM, MacDonald JS, Muggia FM, Henney JE, DeVita JT. Current results of the screening program at the Division of Cancer Treatment, National Cancer Institute. *Eur J Cancer* 1981;17:129–142.
20. Dexter DL, Spremulli EN, Matook GM, Diamond I, Calabresi P. Inhibition of the growth of human colon cancer xenografts by polar solvents. *Cancer Res* 1982;42: 5018–5022.
21. Pessin JE, Bell GI. Mammalian facilitative glucose transporter family: structure and molecular regulation. *Ann Rev of Physiol* 1992;54:911–930.
22. Mehsen JJ. Cytologic and cytochemical techniques for study of viral infections. In: Sonnenwirth AC, Jarrett L, eds. *Gradwohl's clinical laboratory methods and diagnosis*, 8th ed., vol 2. St. Louis: CV Mosby; 1980:2051–2052.
23. Scatchard G. The Attractions of proteins for small molecules and ions. *Ann NY Acad Sci* 1949;5:660–672.
24. Sogin DC, Hinkle PC. Binding of cytochalasin B to human erythrocyte glucose transporter. *Biochemistry* 1980;19:5417–5420.
25. Lavis VR, Lee DP, Shenolikar S. Evidence that forskolin binds to the glucose transporter of human erythrocutes. *J Biol Chem* 1987;262:14571–14575.
26. LeFevre PG, Davis RI. Active transport into the human erythrocyte: evidence from comparative kinetics and competition among monosaccharides. *J Gen Physiol* 1951; 34:515–524.
27. Pardridge WM, Oldendorf WH. Kinetics of blood-brain barrier transport of hexoses. *Biochim Biophys Acta* 1975;382:377–392.
28. Mellanen P, Minn H, Grenman R, Harkonen P. Expression of glucose transporters in head-and-neck tumors. *Int J Cancer* 1994;56:622–629.
29. Weber MJ. Metabolic and transport alterations in cells transformed by rous sarcoma virus. In: Knapp WH, Vyska K, eds. *Current topics in tumor cell physiology and positron-emission tomography*. New York: Springer-Verlag; 1984:1–10.
30. Lin S, Spudich JA. Biochemical Studies on the Mode of Action of Cytochalasin B. Cytochalasin B binding to red cell membrane in relation to glucose transport. *J Biol Chem* 1974;249:5778–5783.
31. Wardzala LJ, Cushman SW. Mechanism of Insulin Action on glucose transport in the isolated rat adipose cell. Enhancement of the number of functional transport systems. *J Biol Chem* 1978;253:8002–8005.
32. Axelrod JD, Pilch PF. Unique cytochalasin B binding characteristics of the hepatic glucose carrier. *Biochemistry* 1983;22:2222–2227.
33. Dick AP, Harik SI, Klip A, Walker DM. Identification and characterization of the glucose transporter of the blood-brain barrier by cytochalasin B binding and immunological reactivity. *Proc Natl Acad Sci USA* 1984;81:7233–7237.
34. Muller WJ, Sinn E, Pattengale PK, Wallace R, Leder P. Single-step induction of mammary adenocarcinoma in transgenic mice bearing the activated c-neu oncogene. *Cell* 1988;51:105–115.
35. Kallinowski F, Vaupel P, Runkel S, et al. Glucose uptake, lactate release, ketone body turnover, metabolic micromilieu and pH distributions in human breast cancer xenografts in nude rats. *Cancer Res* 1988;48:7264–7272.
36. Vaupel P, Fortmeyer HP, Runkel S, Kallinowski F. Blood flow, oxygen consumption and tissue oxygenation of human breast cancer xenografts in nude rats. *Cancer Res* 1987;3496–3503.
37. Fung KP, Choy YM, Chan TW, Lam WP, Lee CY. Glucose regulates its own transport in Ehrlich ascites tumor cells. *Biochem Biophys Res Comm* 1986;134:1231–1237.
38. Haspel HC, Mynarcik DC, Oritz PA, Honkanen RA, Rosenfeld MG. Glucose deprivation induces the selective accumulation of hexose transporter protein GLUT-1 in the plasma membrane of normal rat kidney cells. *Mol Endocrinol* 1991;5:61–72.
39. Shubik P. Vascularization of tumors: a review. *J Cancer Res* 1982;103:211–226.
40. Burant CF, Sivitz WI, Fukumoto H, et al. Mammalian glucose transporters: structure and molecular regulation. *Recent Prog Horm Res* 1991;47:349–388.
41. Gould GW, Thomas HM, Jess TJ, Bell GI. Expression of human glucose transporters in Xenopus oocytes: kinetic characterization and substrate specificities of the erythrocyte, liver and brain isoforms. *Biochemistry* 1991;30:5139–5145.